

Preparation and Modification of Activated Carbon Surface and Functions for Environments



Motoi Machida and Yoshimasa Amano

Contents

1	Pollution of Aquatic Environment	336
2	Adsorbents for Organic Pollutants	336
3	Adsorbents for Ionic Pollutants	340
3.1	Cationic Contaminants	341
3.2	Anionic Contaminants	347
4	Conclusion	362
	References	363

Abstract Preparation and modification of activated carbon (AC) and activated carbon fiber (ACF) were described for the adsorptive removal of contaminants from aqueous phase. For hydrophobic and nonpolar organic pollutants, specific surface area and pore distribution of hydrophobic carbon surface play an important role. On the contrary, hydrophilic carbon surface containing heterolytic oxygen-, nitrogen-, and sulfur-containing functional groups is required for capturing ionic pollutants rather than specific surface area. Carboxy groups was successfully introduced onto carbon surface to remove cationic contaminants as heavy metal cations of Pb^{2+} , Ni^{2+} , Cd^{2+} , Cu^{2+} , etc., while quaternary nitrogen could be formed to some extent on carbon surface for uptaking anionic pollutants of nitrate, phosphate, $Cr_2O_4^{2-}$, AsO_4^{3-} , etc. However, introduction of sulfonic functional groups onto carbon surface for cationic pollutants and alkylamine groups for anionic pollutants has still been challenging subjects.

M. Machida (✉) and Y. Amano
Safety and Health Organization, Chiba University, Chiba, Japan
Graduate School of Engineering, Chiba University, Chiba, Japan
e-mail: machida@faculty.chiba-u.jp; amanoy@faculty.chiba-u.jp

Shunitz Tanaka, Masaaki Kurasaki, Masaaki Morikawa, and Yuichi Kamiya (eds.), 335
Design of Materials and Technologies for Environmental Remediation,
Hdb Env Chem (2023) 115: 335–366, DOI 10.1007/698_2020_673,
© The Author(s), under exclusive license to Springer Nature Singapore Pte Ltd 2020,
Published online: 26 October 2020

Keywords Activated carbon fiber, Adsorption of ionic pollutants, Oxygen- and nitrogen-containing functional groups, Positively charged quaternary nitrogen, Surface chemistry, Textural properties

1 Pollution of Aquatic Environment

In this chapter, porous carbonaceous materials and their surface modification for adsorptive removal of contaminants in aquatic environments were described based on our previous study and some literature survey. Before detail description regarding carbon, char, and fiber, we would like to mention the background of the study to show significance of the developments of new type of porous carbonaceous materials with hetero-atom (N, O, S) functionalized surface.

Pollution of aquatic environment can be defined as contaminations of undesired materials of organic and inorganic compounds found in sea, river, lake, and groundwater. In the pollution of organic materials, not only conventional polycyclic and mono-aromatic organic compounds mainly originated from crude oil but also pesticides and insecticides [1], and nowadays pharmaceuticals and antibiotics [2, 3] are involved for the study field. In regard to inorganic pollutants in aquatic system, heavy metals such as lead (Pb), cadmium (Cd), nickel (Ni), chromium (Cr), arsenic (As), and mercury (Hg) are frequently found worldwide, especially in China, due to rapid urbanization and industrialization [4, 5], and heavy metals penetrated in soil are greatly connected with aquatic environment as well [6–8]. Nitrogen, phosphorous, and potassium are widely known as three main macronutrients, and they are not harmful themselves. But, once excess amounts of nitrogen (ammonia N) and phosphorous (P) are discharged into environment, N and P induce eutrophication of lake (particularly in shallow lake) [9], shallow estuary at coastal area [10], and pollution by nitrate in river [11] and groundwater [12–14]. In this section, relationship between properties of carbonaceous adsorbents and the above various pollutants in water will be described in terms of reduction of the pollution level by adsorptive removal of contaminants.

2 Adsorbents for Organic Pollutants

Carbonaceous adsorbents such as activated carbons/chars and activated carbon fibers have been frequently utilized for the removal of organic compounds from aqueous phase for a long time. Activated carbons consist of a numerous number of curved graphene sheets intertangled each other. Principally, adsorption kinetics is dependent on pore distribution and particle size of adsorbents, and adsorption capacity of organic pollutants is governed by specific surface area and surface nature. For

granular activated chars and carbons, adsorption speed of organic pollutants into pore structure is controlled by diffusion in most of the cases. When we attempt to apply pseudo-first-order and pseudo-second-order kinetics to the experimental data, pseudo-second-order kinetics will be more suitable than pseudo-first-order analysis because pseudo-second-order kinetics is said to be appropriately represented for diffusion controlled mechanism [15–18]. On the contrary, in case of using fine particles of carbonaceous adsorbents including dried leaves, rapid adsorption was observed, and the kinetics obeyed pseudo-first-order kinetics [19] indicating that the rate-limiting step should be collision of the solute onto adsorption sites of the adsorbent surface. The pseudo-first-order kinetics could be also more suitably applied to mesoporous activated carbon than pseudo-second-order for heavy metal adsorption as described latter section [20].

Adsorption capacities of organic compounds on carbon surface are usually proportional to specific surface area of activated char if no or a little oxygen-containing strong acidic surface functional groups are present on the surface. Goto et al. examined the influence of the oxygen species on activated carbon (AC) and found that any sort of oxygen functional group more or less inhibited the adsorption of benzene and nitrobenzene in aqueous solution [21]. Figure 1 shows adsorption isotherms of benzene and nitrobenzene (NBz) on bead-shaped AC (BAC, Kureha Corporation, Japan), AC oxidized with concentrated nitric acid (AC-Ox), and AC-Ox outgassed at 900°C in helium flow (AC-OxOG) together with Langmuir fitting of the isotherms [21]. In case of benzene adsorption, adsorption amount was drastically altered by the oxidation of AC (AC-Ox) from 10 mmol/g to close to zero, while consecutive outgassing treatment led to regaining some amount of capacity. The Langmuir maximum adsorption amounts of 11.4 mmol/g of benzene and 5.5 mmol/g of nitrobenzene on AC are corresponding to the amounts of monolayer coverage of specific surface area of 1,360 m²/g. Significant amount of carboxy groups (3.75 mmol/g by Boehm titration) was introduced to carbon surface by the oxidation, whereas no carboxy groups were detected before the oxidation. The result

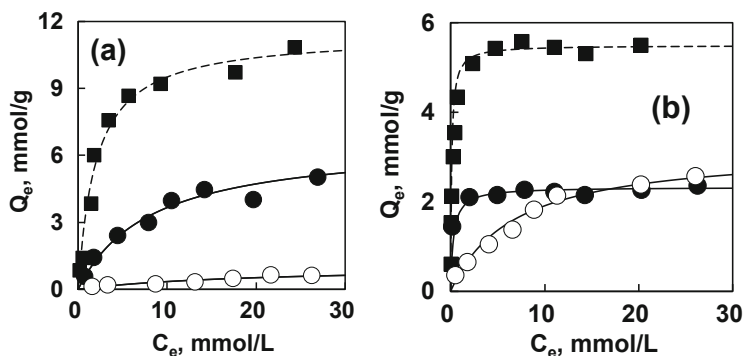


Fig. 1 Langmuir isotherms of benzene (a) and nitrobenzene (NBz) adsorption (b) in aqueous solution onto activated carbon (AC, filled square), AC oxidized with conc. HNO₃ (AC-Ox, open circle) and AC oxidized and outgassed at 900°C (AC-OxOG, filled circle) [21]

implied that the presence of carboxy groups could inhibit the benzene adsorption by the withdrawal of $C\pi$ -electrons on the graphene layer of AC. The decrease in $C\pi$ -electron density could significantly bring the weakness of π - π interaction between AC graphene and benzene by the fact that the amount of basic site was decreased from 0.60 meq/g to 0.00 meq/g (Boehm titration) by the oxidation. Specific surface area was also decreased from 1,360 m^2/g to 140 m^2/g by the oxidation. This is partly caused by physical inhibition by oxygen functional groups such as carboxy, lactone, and phenol groups. But the outgassing treatment at 900°C regained basic site from 0.00 meq/g to 0.48 meq/g, and some amount of benzene could adsorb again on AC-OxOG in Fig. 1. Specific surface area also increased again from 140 m^2/g to 650 m^2/g corresponding to adsorption amount of benzene [21].

As for nitrobenzene (NBz), the adsorption performance was a little different from benzene. Adsorption amount of NBz was not close to zero, but moderate adsorption of NBz could be observed on AC-Ox. The different performance may be caused by difference in dipole moments (D) between benzene and NBz; dipole moment of NBz is 4.22, whereas that of benzene is 0.00. When ACs are oxidized, carbon surface will be altered from hydrophobic to hydrophilic, and then π - π interaction between benzene ring and graphene will be weakened. In case of NBz, adsorption configuration can be estimated to switch from flat-on adsorption via π - π interaction to end-on adsorption via weak electrostatic interaction between NBz and acidic oxygen functional groups. We have not direct evidence for the end-on adsorption of NBz on oxidized BAC(BAC-Ox), but as displayed in Fig. 1b, the adsorption amount of NBz on AC-Ox exceeded that on AC-OxOG at equilibrium solution concentration (C_e) beyond 20 mmol/L in spite of a small specific surface area of only 140 m^2/g of AC-Ox. Ramis et al. examined adsorption of benzene and NBz on TiO_2 , ZrO_2 , and Fe_2O_3 (hydrophilic surface) and observed flat-on orientation for benzene adsorption but side-on (perpendicular) orientation for NBz [22]. This is caused by strong π -electron withdrawal effect by nitro group in NBz. Chen et al. also observed the alternation of adsorption orientation of phenyl hydroquinone (PHQ) on graphene nanoplatelets from Langmuirian flat-on at low concentration and then to endwise orientation at higher PHQ concentration in aqueous phase [23].

As long as strong oxygen functional groups like carboxy groups are not present in graphene structure of ACs, the adsorption amount of mono-aromatics will be approximately proportional to specific surface area due to the mechanism of mono-layer Langmuir-type adsorption with π - π interaction between benzene ring and graphene. When we use granular activated carbon (GAC) and remove large organic molecules such as dyes dissolved in aqueous phase, larger pore diameter is needed to accommodate the pollutants. Figure 2 represents adsorption performance of small (NBz, mono-aromatics) and large (tannic acid) molecules to ACs as a function of mesopore volume [24]. Normally ACs are rich in micropore and have hydrophobic graphene surface; therefore, they are suitable for small organic molecules as mono-aromatics. The adsorption amounts of mono-aromatics are usually proportional to specific surface area and/or micropore volume. However, large bulky molecules as tannic acid can adsorb only larger pore surface as mesopore and macropore. As clearly shown in Fig. 2, although the amounts of nitrobenzene

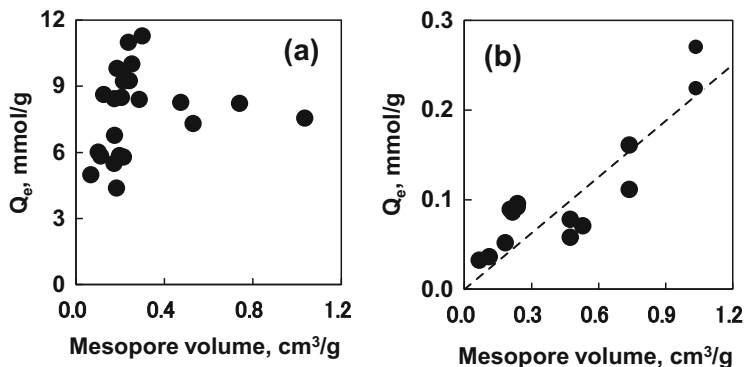


Fig. 2 Adsorption amount of nitrobenzene (NBz) (a) and tannic acid (b) as a function of mesopore volume of various modified activated carbons (ACs) [24]

adsorption exhibit poor relationship with mesopore volume, those of tannic acid uptake have a good relationship with mesopore volume [24]. Large bulky molecules as dyes and tannic acid dissolved in water have ionic parts in their molecules; therefore, large pore size is more important to capture them for AC structure than small molecules. Mono-aromatics rather adsorb via π - π interaction (HOMO-LUMO system) between aromatics adsorbates (MOMO) and carbon adsorbents (LUMO) [25]. In adsorptive removal of organic contaminants in water, the following conditions may be essential for activated chars and their surface:

- (a) Some amount of specific surface area will be needed, probably at least 500 m²/g.
- (b) Oxygen content should be minimized in the carbonaceous adsorbents at any stage of production, storage, practical usage, and regeneration because oxygen functional groups, particularly carboxy groups, always cause poor adsorption behavior for the organic pollutants. Carbon materials can accumulate oxygen in air even at the ambient conditions, and then the surface will be gradually degraded with time.
- (c) Adsorption speed is controlled by diffusion of organic contaminants in the pore structure, and then fine powder and/or mesoporous structure will be required for increasing the adsorption speed especially in aqueous phase. For example, fine activated carbon powder was sprayed at the outlet of exhaust gas to even capture gas phase dioxins in the waste incineration plant in Japan.

Since removal of organic pollutants has been a major role of activated carbons (ACs) for a long time, above conditions for organic pollutants were fully satisfied in the commercial production base of activated carbons (commercially available ACs), thanks for the efforts in industries. Ideally when activated carbon (AC) and activated carbon fiber (ACF) are composed of carbon and hydrogen and condensed poly aromatic ring is formed, the size of graphene structure can be estimated as shown in Fig. 3 [26]. Using the simple model, chemical formula and the number of benzene ring can be easily estimated as an ideal case; e.g., if only 99.8 wt% carbon and 0.2 wt

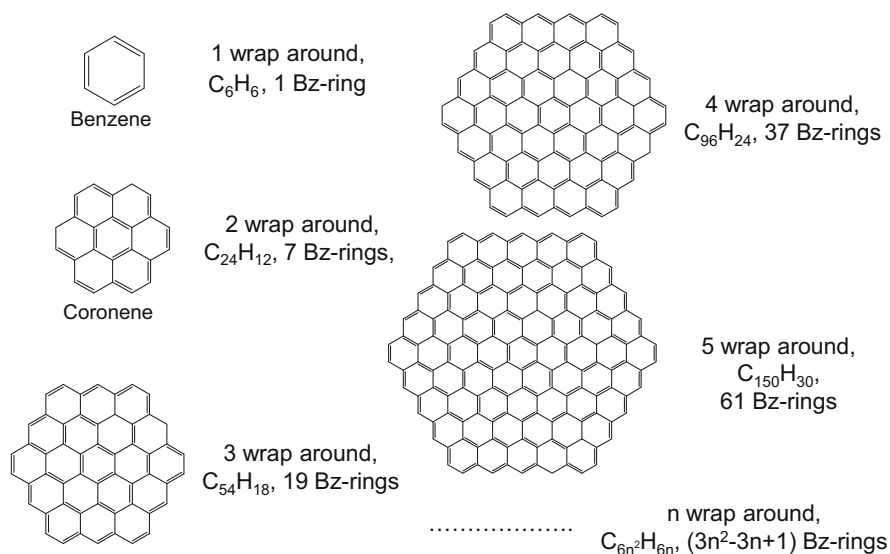


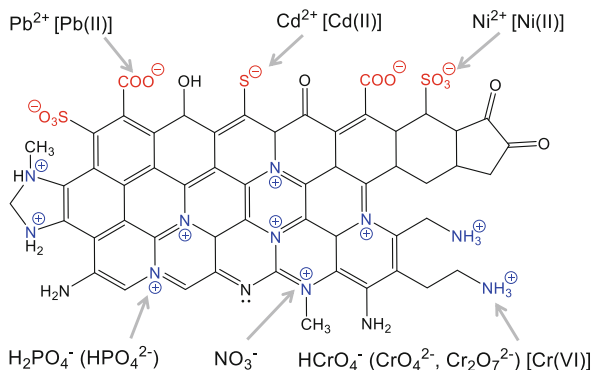
Fig. 3 Model of unit crystal graphene size of activated carbon (AC) [26]

% hydrogen are contained in AC or ACF, we can obtain chemical formula of C₁₀₀₀₀₀₀H₂₅₀₀ and the number of benzene ring per one graphene sheet of 5.2×10^5 . In practice, graphene sheet is not flat because curved three-dimensional graphene unit structure containing 5 and 7 membered rings and heterolytic atoms as oxygen, nitrogen, and sulfur must be formed [27]. The porous structure is constructed by the curved structure of graphene units; otherwise, all graphene sheets become two dimensional with only sp² hybrid bonds (no sp³ hybridization), and then graphene sheets are binding each other resulting in little porous structure (small specific surface area).

3 Adsorbents for Ionic Pollutants

There are various ionic pollutants in water environment such as heavy metals, halogens, oxoacids, and some kinds of dyes. For adsorptive removal of the ionic pollutants, ion-exchange resins [28] and metal oxides [29] have been utilized, but carbonaceous materials can be used as well if suitable carbon surface modifications can be made [26]. In this chapter, applicability of carbonaceous adsorbents of ACs and ACFs for the removal of ionic contaminants in aqueous phase together with current developments of new carbon/char adsorbents with heteroatom functions. Some of them are successfully developed superior to ion-exchange resins, and the others are under the development in the laboratory scale. Figure 4 displays the

Fig. 4 Some surface functions on graphene layer required to effectively capture cationic and anionic contaminants from aqueous phase [30]



concept of the modification on the heteroatom functionalized carbonaceous adsorbent [30].

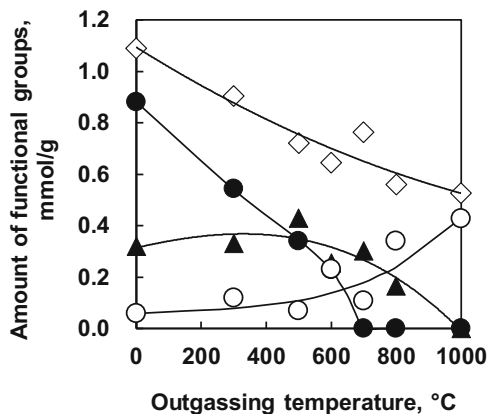
3.1 Cationic Contaminants

3.1.1 Surface Functional Groups for Cations

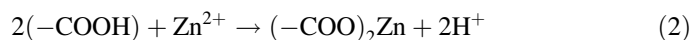
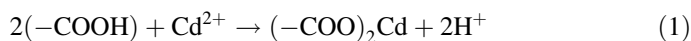
As represented in Fig. 4, carboxy ($-\text{COO}^- \text{H}^+$, $-\text{COO}^- \text{Na}^+$), sulfonic ($-\text{SO}_3^- \text{H}^+$, $-\text{SO}_3^- \text{Na}^+$), and thiol ($-\text{S}^- \text{H}^+$, $-\text{S}^- \text{Na}^+$) groups on carbon are widely proven to be effective for the adsorption of cationic pollutants, such as lead(II) (Pb^{2+}), cadmium (II) (Cd^{2+}), nickel(II) (Ni^{2+}), and Cs(I) (Cs^+) dissolved in water. Weakly negatively charged $\text{C}\pi$ site is working as well for the adsorption sites of heavy metal ions. Carboxy groups can be introduced to the carbon surface with oxidation by H_2O_2 , HNO_3 , and $(\text{NH}_4)_2\text{S}_2\text{O}_8$ [31], whereas it is hardly achieved that sulfonic acid can be individually introduced on graphene layer of ACs although several attempts have been done [32, 33]. Thiol functional groups ($-\text{SH}$) on carbon surface are also applicable especially for the capture of cadmium(II) [34]. Thiol groups may be more suitable for cadmium(II) uptake than for lead(II) on mesoporous silica materials, while carboxy groups on carbon are better for lead(II) than for cadmium (II) [35]. Assuming that thiol groups ($\text{Ar}-\text{S}^- \text{H}^+$) could work as soft base and carboxy groups ($\text{Ar}-\text{COO}^- \text{H}^+$) as hard base according to HSAB theory for Lewis acids and bases, the pair of soft acid of cadmium ion (Cd^{2+}) and soft base of thiol groups ($\text{Ar}-\text{S}^-$) and that of medium acid of lead ion (Pb^{2+}) and hard base of carboxy groups ($\text{Ar}-\text{COO}^-$) should be better combination than the opposite pairs of the heavy metals and the surface functional groups.

In practice, the introduction of carboxy groups is probably the most feasible for the modification of carbon surface to remove heavy metal cations. The amounts of carboxy groups can be ultimately introduced with the order of $(\text{NH}_4)_2\text{S}_2\text{O}_8 > \text{HNO}_3 > \text{H}_2\text{O}_2$. In case of using HNO_3 as an oxidant, mixture of activated carbon (AC) and concentrated HNO_3 is boiled generating blown colored NO_2 gas as the oxidation progressed, and

Fig. 5 Surface oxygen-containing acidic functional groups and basic sites ($C\pi$ sites) of HNO_3 oxidized AC as a function of outgassing temperature from 300°C to 1,000°C. The functional groups were determined with Boehm titration; carboxy groups (filled circle), lactone groups (filled triangle), hydroxy groups (open diamond), basic sites (open circle) [36]



acidic oxygen function as carboxy and lactone groups can be introduced on AC surface. Figure 5 shows the changes in oxygen functional groups and basic sites on activated carbon (AC) oxidized with 6 M HNO_3 and their outgassed materials [36]. And Fig. 6 represents corresponding adsorption amounts of cadmium(II) and zinc(II) cations and the ratio of discharged proton (H^+) over adsorbed cadmium(II) and zinc(II), respectively [36]. By the oxidation of AC, significant amounts of carboxy ($-COOH$), lactone ($-OCO-$), and hydroxy ($-OH$) groups were introduced and gradually decreased in carboxy and hydroxy groups by increasing outgassing temperature, and the carboxy groups were disappeared until 700°C (Fig. 5). In contrast, basic sites ($C\pi$ sites) were increased as electron withdrawal carboxy functions were decreased. On the other hand, the lactone groups exhibit relatively constant values until 700°C indicating that lactone groups can be converted to CO/CO_2 by decomposition, while a part of lactone can be newly generated by dehydration of carboxy and hydroxyl groups. As clearly seen in Fig. 6, the adsorption of cadmium(II) and zinc(II) was taken place with ion-exchange mechanism because two protons were discharged, while one divalent metal(II) cation was adsorbed when more than the stoichiometric amount of carboxy groups was available on carbon surface as shown in Fig. 5.



Contrarily when most of carboxy groups were removed from graphene layers as CO/CO_2 and H_2O , and/or converted to lactone on the graphene, adsorption mechanism was switched from ion-exchange mechanism (Eqs. (1) and (2)) to electrostatic interactions between heavy metal cations and $C\pi$ -electrons on the graphene that could have slightly negative charged properties. Similar electrostatic interactions could be observed for lead(II) adsorption [37]. Electron density of $C\pi$ sites could be corresponding to basic sites of Boehm titration as also displayed in Fig. 5. The electron density might be able to be easily reduced by electron withdrawing groups

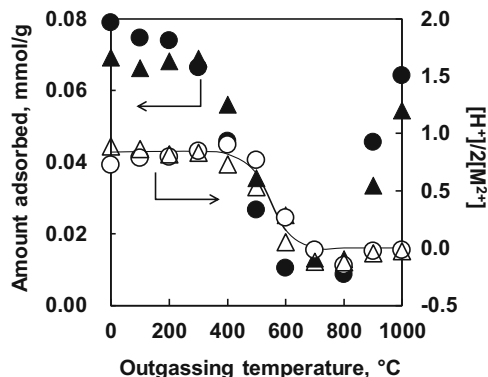


Fig. 6 Adsorption amounts of cadmium(II) (filled circle) and zinc(II) (filled triangle) as a function of outgassing temperature from 100°C to 1,000°C, corresponding molar ratios of discharged proton (H^+)/adsorbed cadmium(II) (open circle) and zinc(II) (open triangle) ($[H^+]/2[M^{2+}]$) in which $[H^+]/2[M^{2+}]$ is 1.0 and 0.0 which represent ion-exchange mechanism and $C\pi$ sites adsorption, respectively [36]

of carboxy and lactone at the edge of graphene layer, but the $C\pi$ electron density might be increased by the reduction of them leading to the rise in the adsorption amounts of metal cations as could be seen in Fig. 6.

When greater amounts of heavy metal cations should be accommodated in ACs and ACFs, oxidation with ammonium peroxodisulfate (APS, $(NH_4)_2S_2O_8$) solution is one of the most effective options to introduce abundant amounts of oxygen functional groups [38, 39]. The APS oxidation can be conducted using ambient temperature, although a few days or longer will be required to generate enough carboxy groups on AC and ACF surface. Effective carboxy groups can be formed on carbon surface by destructing the graphene edges and whole graphene basal plane. Figure 7 shows changes in adsorption amounts of lead(II) cation (Pb^{2+}) as a function of APS oxidation time [38]. The adsorption amount of lead(II) is greatly improved from only 0.1 mmol/g (non-oxidized BAC) to as much as 2.3 mmol/g (ca. 0.5 g-lead (II)/g-AC oxidized). On the other hand, specific surface area (S_{BET}) was unilaterally declined during the oxidation as represented in Fig. 8 in which maximum adsorption amounts of day 4 (30°C oxidation) and day 8 (20°C oxidation) were consistent with the days losing their specific surface area (close to zero) [38]. The results indicated that carboxy groups available for lead(II) adsorption could reach the maximum after measurable porous structures were completely destroyed (Fig. 8). As shown in Fig. 9 [38], carbon content was decreased from 94% down to 65% within first 2 days, whereas oxygen was increased from 5% up to 35%, but after that the adsorption amounts of lead(II) went up until day 4 (30°C oxidation) and day 8 (20°C oxidation) revealing that oxygen functional groups would be introduced by forming precursors of carboxy groups (hydroxyl and/or carbonyl, etc.) until day 2 and then they might be further converted to carboxy groups that were only effective function for the adsorptive removal of heavy metal cations. Adsorption amount of lead(II) can be

Fig. 7 Increase in the adsorption amounts of lead (II) (Pb^{2+}) as a function of oxidation time. Starting materials; beaded-shaped activated carbon (BAC, Kureha Corporation). Oxidation with ammonium peroxodisulfate ($(\text{NH}_4)_2\text{S}_2\text{O}_8$) solution at 20°C (filled circle) and 30°C (filled triangle). Solution equilibrium pH (pH_e) > 4.0 . Initial lead (II) concentration; 4.8 mmol/L [38]

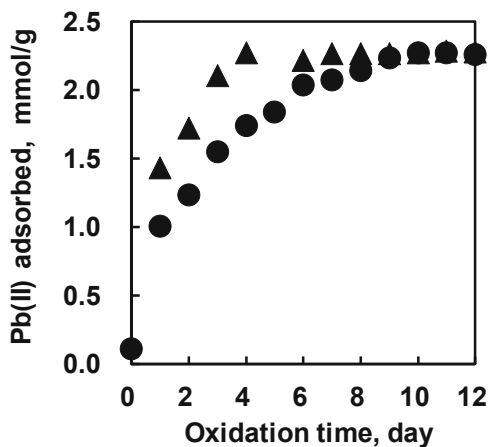


Fig. 8 Decrease in B.E.T. specific surface area of BAC from $1,380 \text{ m}^2/\text{g}$ to less than $25 \text{ m}^2/\text{g}$ during oxidation in peroxodisulfate ($(\text{NH}_4)_2\text{S}_2\text{O}_8$) solution at 20°C (filled circle) and 30°C (filled triangle) [38]

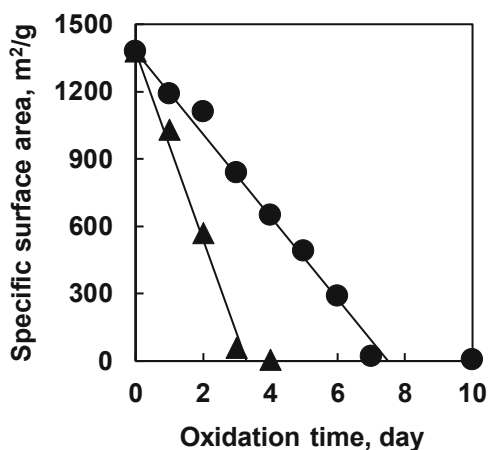


Fig. 9 Changes in carbon (filled circle and triangle) and oxygen (open circle and triangle) content during oxidation in peroxodisulfate ($(\text{NH}_4)_2\text{S}_2\text{O}_8$) solution at 20°C (open circle) and 30°C (open triangle) [38]

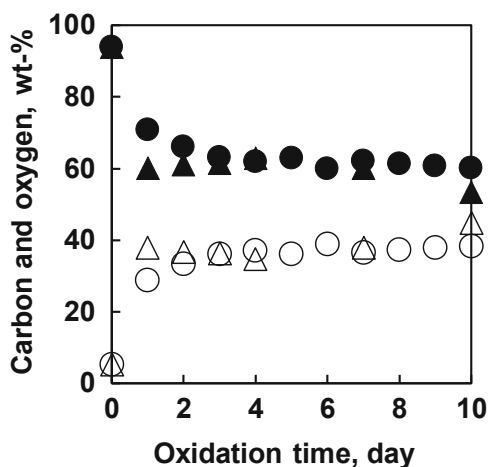
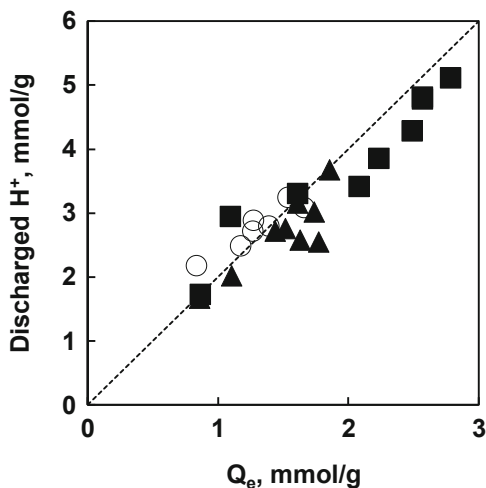


Fig. 10 Relationship of the proton discharged into water (H^+ [mmol/g]) and the amount of lead(II) (Pb^{2+}) adsorbed onto oxidized activated carbon fiber (Q_e [mmol/g]) by ion-exchange process. Oxidized ACF (KF1500) by $(NH_4)_2S_2O_8$ (filled triangle and square), carboxy functionalized ion-exchange resin (open circle) [39]



significantly improved for activated carbon fiber (ACF) by the oxidation with ammonium peroxodisulfate (APS, $(NH_4)_2S_2O_8$) as well. Figure 10 shows an evidence of ion-exchange mechanism for the adsorption of lead(II) onto oxidized ACF (Toyobo Co., Ltd., Japan) and carboxy functionalized ion-exchange resin (AMBERLITE™ IRC86) [39]. When one lead(II) cation is uptaken on the adsorbents, two protons (H^+) are instead released from carboxy groups ($-COO^-H^+$) into water, supporting ion-exchange mechanism. However, only 4.01 mmol/g of carboxy groups was measured by Boehm titration despite as much as 2.79 mmol/g of lead (II) (Pb^{2+}) adsorbed. The results reveal that an excess amount ($2.79 \times 2 - 4.01 = 1.57$ mmol/g) of lead(II) could adsorb on the oxidized ACF. We are not sure, but some unknown sites may participate in the adsorption via ion-exchange. In both AC and ACF, APS oxidation leads to the destruction of carbon structure introducing nearly a half portion of oxygen in the total elemental composition. Oxidized AC and ACF with the abundant oxygen are easily dissolved in the basic solution (e.g., NaOH solution), thereby the extent of oxidation should be controlled not to be dissolved in a practical use [38, 39], although much amount of carboxy groups can be easily introduced onto graphene layers for AC and ACF. In our oxidation procedure, 2 M (mol/L) APS ($(NH_4)_2S_2O_8$) in 1 M H_2SO_4 solution was mixed with AC (or ACF) at APS solution/AC ratio of 50 mL/g or more at 20–30°C [38]. The 2 M APS solution and the mixing ratio of 50 mL/g-AC were most important points to introduce sufficient amounts of carboxy groups ($-COOH$) introduced onto graphene layer of ACs and ACFs. Since higher oxidation temperature and longer oxidation period also cause the destruction of graphite structure of AC and ACF, the temperature and period of APS oxidation should be suitably adjusted depending on the properties of each AC and ACF [40].

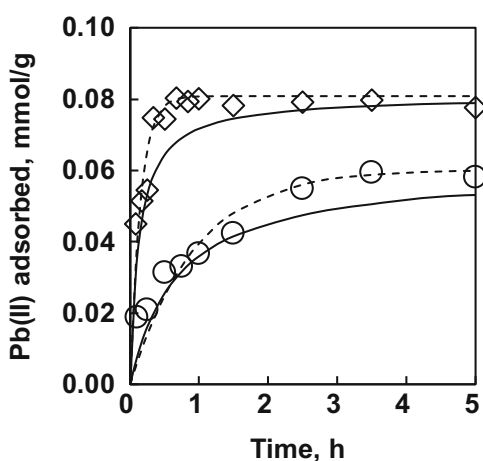
In addition, even if AC surface can be successfully filled with carboxy groups by the oxidation, as increase in the adsorption amount of heavy metal cations, pH of aqueous solution will be decreased less than 4 by discharging corresponding

amounts of protons (Fig. 10) resulting in stopping further adsorption caused by competitive adsorption of abundant amounts of protons. Thereby, protons of carboxy groups ($-\text{COO}^{-}\text{H}^{+}$) should be replaced by sodium ions in NaCl/NaOH solution forming $-\text{COO}^{-}\text{Na}^{+}$ as well as ion-exchange resin from the practical points of view.

3.1.2 Adsorption Kinetics

Not only adsorption capacity but adsorption kinetics is an important aspect from the practical point of view. In general, fine powder AC exhibits much faster adsorption speed than granular AC. However, fine powder has disadvantage because it is hard to be recovered after use for regeneration. On the other hand, pseudo-second-order kinetics can be observed for granular AC in which diffusion control kinetics is progressed [16]. To increase kinetic efficiency of granular AC, mesoporous and/or macroporous AC should be prepared. As mentioned in the previous section, mesoporous granular ACs were prepared from bamboo chips and measured adsorption kinetics of lead(II) as displayed in Fig. 11 [20] in which pseudo-first-order kinetics rather than pseudo-second-order was fitted to the experimental results, indicating that adsorption process was controlled by not diffusion in the porous structure but collision to the adsorption sites in which no sterically restriction in approaching the adsorption sites occurred. In this case, since non-oxidized AC was examined ($\text{C}\pi$ sites), oxidized mesoporous AC (carboxy groups) has not been clarified for kinetics yet. But, as long as we have examined, pseudo-second-order kinetics is more applicable for oxidized ACF which is microporous one before oxidation [39] and for most of other oxidized ACs and ACFs.

Fig. 11 Adsorption kinetics of lead(II) on mesoporous activated carbons (ACs) derived from bamboo chips (BC). ZnCl_2/BC ratio of 1.0 (open circle) and 6.0 (open diamond) in activation at 500°C . Dashed and solid lines represent the approximation curves by pseudo-first-order and pseudo-second-order kinetic models, respectively. Initial lead(II) concentration; 0.48 mmol/L [20]

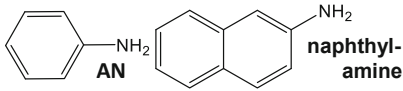
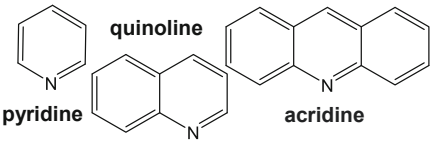
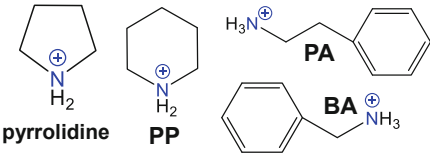
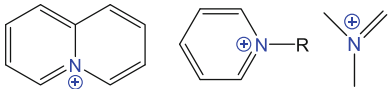


3.2 Anionic Contaminants

3.2.1 Surface Functional Groups/Sites (Nitrogen and C π Sites) for Anions

Sodium, chloride, and hydroxy ions are not regarded as pollutants, but not only fluoride, bromide, arsenic, and chromate but also nitrate and phosphate are also regarded as contaminants in aqueous phase to be removed as mentioned in the previous section. For the adsorption of cationic pollutants, oxygen-containing (carboxy) and sulfur-containing (sulfonic and thiol) groups are effective to capture Cs^+ , Pb^{2+} , Cd^{2+} , Ni^{2+} , Cu^{2+} , etc., while for adsorptive removal of anionic pollutants, nitrogen-containing functions on the adsorbents are said to be desirable to attract anionic impurities as F^- , Br^- , H_2AsO_4^- , HCrO_4^- , $\text{Cr}_2\text{O}_7^{2-}$, NO_2^- , NO_3^- , H_2PO_4^- , etc. Table 1 displays some typical nitrogen-containing compounds and their nitrogen hybridization (sp^2 , sp^3 orbital) and pK_a range that represents the degree of affinity to protons (H^+) in aqueous phase. Aromatic amine (aniline, pK_a 3–5)- and pyridine (pK_a 5–7)-type nitrogen species (N-6) cannot accept protons at pH above 7, and they are negatively charged around neutral to basic region implying that repulsive force is working between anionic pollutants and carbon surface. Alternatively, aliphatic amine ($\text{pK}_a > 9$) and quaternary nitrogen species (N-Q) are positively charged in a wide range of solution pH. The aliphatic amine types can easily attract protons (H^+)

Table 1 Nitrogen hybridization and pK_a ranges of nitrogen-containing compounds assuming solution pH 7–8

Nitrogen-containing compound	Nitrogen hybridization	pK_a range
 AN naphthyl-amine	sp^3	3–5
 pyridine quinoline acridine	sp^2	5–7
 pyrrolidine PP PA BA	sp^3 (Aliphatic amines)	9<
 quaternary nitrogen (N-Q) family	sp^2 (N-Q)	Positively charged

Prepared using the data in refs. [41, 42]

from weak acidic to weak basic region [41, 42]. They are sometimes detected on carbon surface. Dioum and Hamoudi examined nitrate adsorption onto mesoporous silica materials functionalized with propyl-ammonium (alkyl amine) and propyl-*N,N,N*-trimethylammonium (N-Q) and observed effective progress in adsorption on the surface nitrogen species in which nitrate (NO_3^-) adsorption capacities of 0.9–1.0 mmol/g-adsorbent were achieved [43]. On the carbonaceous materials, such sufficient amount of effective nitrogen has not been introduced yet. Other than effective nitrogen species of alkyl amine and quaternary nitrogen (N-Q), $\text{C}\pi$ electrons on graphene layers play a role of nitrate adsorption as well as heavy metal cations because $\text{C}\pi$ electrons can accommodate protons at acidic region (pH 3–5) and the positively charged surface attracts nitrate anion. In the same way of the adsorption of heavy metal cations, $\text{C}\pi$ electrons can show their ability only in the absence of electron-withdrawing oxygen functional groups. Figure 12 shows adsorption isotherms of nitrate on de-ashed activated carbon (AC, Calgon F400) and ACs oxidized and outgassed at 600°C and 900°C, respectively [44]. The properties of adsorbents including oxidized AC are tabulated as well in Table 2 [44]. The de-ashed AC adsorbed nitrate by 0.1 mmol/g. The de-ashed AC was oxidized with 8 M HNO_3 solution at 95°C to introduce acidic oxygen functional groups, washed with pure water using Soxhlet extractor, and calcined in air for 6 h to completely decompose the nitrate ions remained in the carbon. The oxidized AC was referred to as Ox in Table 2. Ox was outgassed by heat treatment in inert gas at 600°C (Ox-6OG) and 900°C (Ox-9OG) to remove oxygen as CO/CO_2 and H_2O [45]. There are some amounts of carboxy and lactone groups in de-ashed AC (F400). The acidic oxygen functional groups increased by oxidation (Ox). We could not observe any nitrate adsorption on Ox revealing that acidic oxygen functional groups of carboxy and lactone might withdraw $\text{C}\pi$ electrons on graphene layers leading to inhibiting nitrate adsorption. Some adsorption occurred on Ox-6OG, but the adsorption amounts were less than those of F400 because carboxy and lactone groups on Ox-6OG were considerably reduced from those on Ox, but they are greater than F400. No detection

Fig. 12 Adsorption isotherms of nitrate on activated carbons (AC, F400) at 25°C. Original de-ashed F400 AC (open square, Ox), oxidized F400 and outgassed at 600°C (filled triangle, Ox-6OG), and oxidized F400 and outgassed at 900°C (filled circle, Ox-9OG) [44]

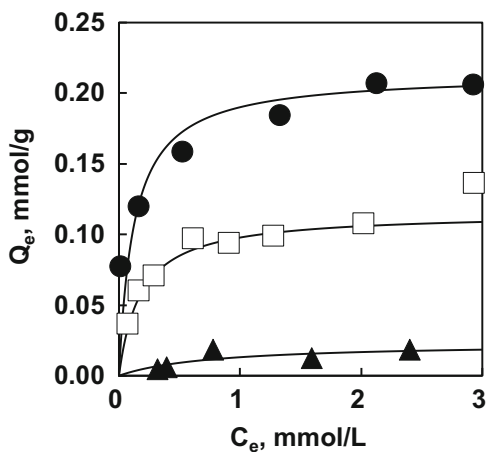


Table 2 Textural, bulk, and surface properties for F400-activated carbon (AC) and modified ACs [44]

AC	Surface area and pore volumes			Elemental composition			Surface functional groups/sites ^a					
	S _{ges} m ² /g	V _{total} cm ³ /g	V _{micro} cm ³ /g	V _{meso} cm ³ /g	Carbon, wt%	Hydrogen, wt%	Nitrogen, wt%	Oxygen ^b , wt%	Carboxy, mmol/g	Lactone, mmol/g	Phenol, mmol/g	Basic sites, mmol/g
F400 ^c	1,290	0.612	0.421	0.191	90.8	0.1	0.6	8.5	0.15	0.13	0.32	0.29
Ox	820	0.406	0.223	0.183	80.2	0.2	0.9	18.8	0.90	0.52	1.19	0.06
Ox-6OG	1,110	0.665	0.446	0.219	90.0	0.3	0.9	8.9	0.27	0.29	0.67	0.21
Ox-9OG	1,120	0.666	0.467	0.199	95.2	0.2	1.2	3.5	0.00	0.00	1.04	0.27

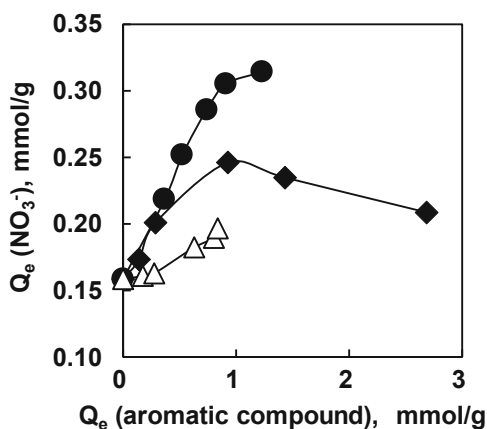
^aMeasured by Boehm titration^bCalculated by difference^cF400: de-ashed Filtrasorb 400

of carboxy and lactone groups and the largest adsorption amount of nitrate could be observed for Ox-9OG. Thereby, the amounts of carboxy and lactone groups might be adversely proportional to the adsorption amounts of nitrate.

3.2.2 Surface Nitrogen (Alkyl Amine Type)

As shown in Table 1, alkyl amine type of nitrogen such as benzylamine (BA), phenethylamine (PA), and piperidine (PP) can accommodate protons (H^+) in a wide range from acidic to weak basic region (solution $pH < 9$) [41, 42]. Although adsorption capacity of $C\pi$ electrons sites is greatly influenced by solution pH , principally alkyl amines are always positively charged as long as pH is less than 9. For the present, alkyl amines have never been detected on carbon surfaces. Alternatively, mono-aromatic amine compounds were mixed with solution to inspect the effect of the amines on the adsorption of nitrate onto AC surface. Figure 13 represented the possibility of the effectiveness of alkyl amine on the carbon for nitrate adsorption [46]. The adsorption of nitrate was conducted in the presence of aniline (AN), benzylamine (BA), and phenethylamine (PP). Comparing to absence of the amines, co-existence of the molecular amines in aqueous phase could improve the adsorption amount of nitrate. The enhancement of nitrate adsorption was most pronounced for phenethylamine and then benzylamine and slightly effective of aniline. The order of the effectiveness is consistent with pK_a values (acidity) of phenethylamine (pK_a 9.83) > benzylamine (9.33–9.34) > aniline (4.87) [41, 42]. The results were supported by the fact that the propyl-ammonium (alkyl amine, $R-NH_2$) on mesoporous silica materials became suitable adsorption sites as well [43], whereas aromatic amine like aniline in which amine groups were directly bound to aromatic ring (aromatic amine, $Ar-NH_2$) cannot be effective function to capture nitrate anion. Consequently, improvement of nitrate adsorption might be promising for ACs if amine groups possessing pK_a values greater than 9, e.g., benzylamine, phenethylamine, and piperidine, can be successfully introduced on the carbon surface.

Fig. 13 Adsorption of nitrate on activated carbon (AC, de-ashed F400) at 25°C in the presence of aniline (AN, open triangle), benzylamine (BA, filled diamond), and phenethylamine (PA, filled circle). Equilibrium solution pH (pH_e) 2.0, initial concentration of chloride $[Cl]_0$: 30 mM [46]



In addition to anionic pollutants, alkyl amine function, in the case of mesoporous silica materials, is useful for cationic pollutants such heavy metal ions as cadmium(II) and lead(II) in neutral and basic region (solution pH > 7–8) in which lone pair of nitrogen atom in amine groups can preferably accommodate cationic ions as well as protons (H^+) by forming covalent bond with the lone pair of nitrogen [47, 48]. Therefore, alkyl amine functionalized carbon can be utilized for adsorptive removal of both anions (acidic and neutral region) and cations (neutral and basic region) when it will be successfully prepared in the future as well as mesoporous silica materials.

3.2.3 Surface Nitrogen (Quaternary Nitrogen, N-Q)

In our previous study, the introduction of alkyl amine, piperidine, and quaternary nitrogen (N-Q) was attempted. In the several trials, only quaternary nitrogen (N-Q) has been able to be doped on the carbonaceous adsorbents to some extent. According to the procedure of the research group in Pennsylvania State University in which AC was oxidized first and then ammonia gas treated at $700^\circ C$ [49], bead-shaped activated carbon (BAC, Kureha Corporation) was oxidized with APS ($(NH_4)_2S_2O_8$) solution followed by ammonia gas treatment at $950^\circ C$ and then supplied for adsorption experiment of nitrate [50]. In our study, ammonia treatment temperature was altered from $700^\circ C$ (Penn State temperature) to $950^\circ C$ due to thermodynamically favorable temperature to form quaternary nitrogen (N-Q) at $950^\circ C$ referring to the study by Pel et al. [51]. In principle, carbonization is the endothermic reaction of dehydrogenation releasing hydrogen and oxygen as CO/CO_2 and H_2O and also nitrogen and sulfur as ammonia and hydrogen sulfide. Rising treatment temperature, transformation of pyrrolic nitrogen (N-5) to pyridinic nitrogen (N-6) is firstly taken place, and then condensation of carbon matrix will be progressed to spread graphene unit together with incorporation of nitrogen as N-Q ($=N^+<$) in the graphene layers as a result [51]. Figure 14 represents adsorption isotherms of nitrate on as-received AC (BAC) and AC oxidized followed by

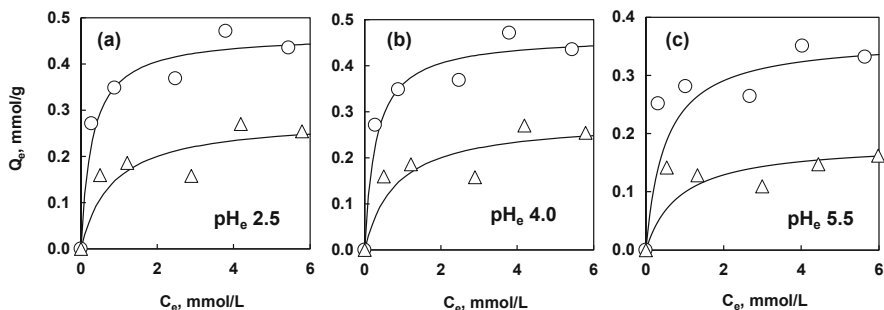


Fig. 14 Langmuir isotherms of nitrate adsorption on as-received AC (open triangle) and oxidized and ammonia gas-treated ($950^\circ C$) AC (open circle) in ambient temperature at equilibrium solution pH (pH_e) 2.5 (a), 4.0 (b), 5.5 (c) [50]

ammonia treated AC (Ox-9.5AG) as a function of equilibrium solution pH (pH_e) 2.5–5.5 [50]. The as-received AC has neither acidic oxygen groups nor nitrogen species, and then all adsorption sites are estimated to be $C\pi$ sites, thereby adsorption amounts of nitrate increase with lowering pH_e due to larger proton concentration at low pH_e indicating that more positively charged surface can attract nitrate anion. The difference between as-received AC and Ox-9.5AG could be attributed to the difference in N-Q content introduced to Ox-9.5AG. The specific surface area of AC ($1,380 \text{ m}^2/\text{g}$) is much larger than Ox-9.5AG ($770 \text{ m}^2/\text{g}$) also supporting that N-Q sites on Ox-9.5OG can play a specific role for the greater nitrate adsorption [50].

A high nitrogen content material of melamine form was also supplied for the preparation of nitrogen-containing carbonaceous adsorbent. Melamine sponge (ML, Fuji Gomu Co., Ltd.) was impregnated with ZnCl_2 solution (ML to ZnCl_2 ratio of 3 and 6), dried at 110°C , and activated at 500°C [52]. The carbonized materials were named as Z3 and Z6. Specific surface area of the melamine sponge (ML) was only $1 \text{ m}^2/\text{g}$, but it improved by the ZnCl_2 activation to 58 and $99 \text{ m}^2/\text{g}$ for Z3 and Z6, respectively. The Z3 and Z6 were further treated with methyl iodide (CH_3I) to principally convert N-6 remaining on Z3 and Z6 to N-Q (Z3-Q and Z6-Q) via nucleophilic substitution reaction ($\text{S}_{\text{N}}2$) as displayed in Eq. (3).

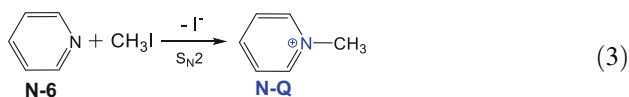


Figure 15 shows the results of screening test of nitrate adsorption on the melamine form-derived carbonaceous materials [52]. Surprisingly starting material of melamine form itself adsorbed nitrate ion to some extent even though specific surface area was only $1 \text{ m}^2/\text{g}$ (0.1% of usual values of ACs). We are not sure but nitrogen species and/or some sponge structure may contribute to the adsorption. The

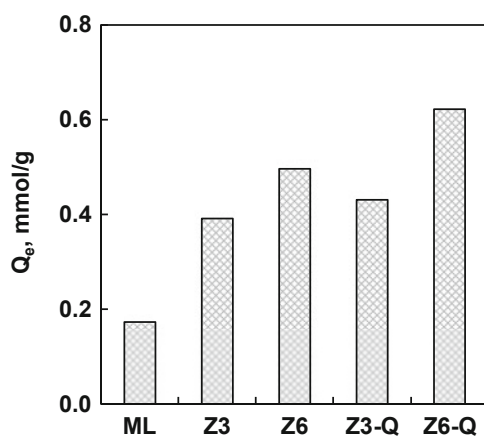


Fig. 15 Adsorption of nitrate on melamine sponge (ML), ML activated with ZnCl_2 at 500°C by ML/ ZnCl_2 ratio of 3 and 6 (Z3, Z6) and their CH_3I treated (N-6 to N-Q converted) materials (Z3-Q, Z6-Q). Initial nitrate concentration: 200 mg/L , equilibrium solution pH (pH_e) 3–4 [52]

Fig. 16 Adsorption isotherms of nitrate on ZnCl_2 activated melamine sponge (Z6, open circle) and post- CH_3I -treated Z6 to convert N-6 to N-Q (Z6-Q, filled circle). Equilibrium solution pH (pH_e) 3–4 [52]

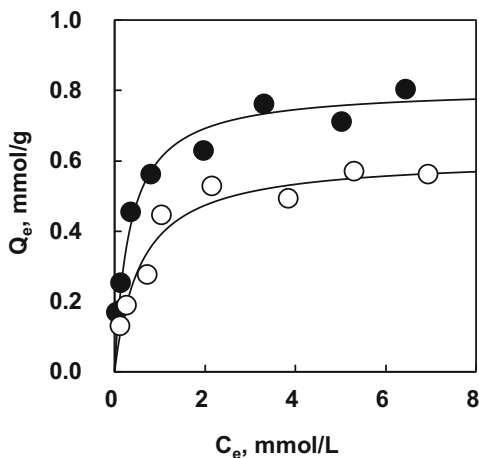
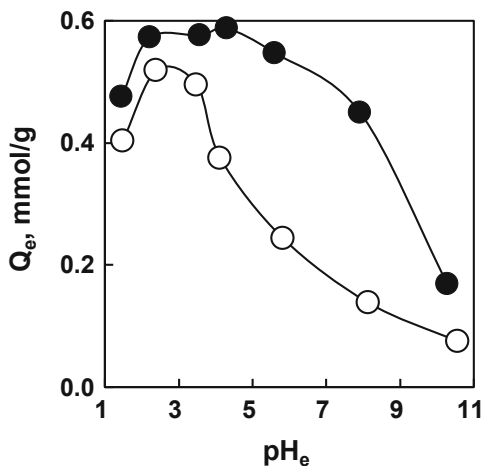


Fig. 17 Influence of equilibrium solution pH (pH_e) on the adsorption of nitrate onto ZnCl_2 -activated melamine sponge (Z6, open circle) and post- CH_3I -treated Z6 to convert N-6 to N-Q (Z6-Q, filled circle) [52]

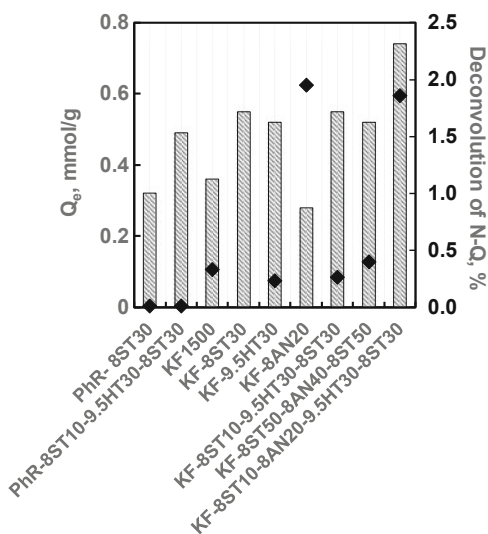


ZnCl_2 activation improved nitrate adsorption from 0.2 mmol/g to 0.4–0.5 mmol/g for Z3 and Z6. Post methyl iodide (CH_3I) reaction could slightly increase the nitrate adsorption amount for Z6. As representing adsorption isotherms of nitrate on Z6 and Z6-Q in Fig. 16 [52], Z6-Q is superior to Z6 at equilibrium solution pH (pH_e) 3–4 probably due to greater amount of quaternary nitrogen (N-Q) on Z6-Q. The above estimation was supported by Fig. 17 [52] because Z6-Q maintained the adsorption amounts of nitrate ranging pH_e 2–8, but steep decline of nitrate adsorption was observed from pH_e 4 to 8 for Z6 sample. The results implied that constant positively charged N-Q could be dominant on Z6-Q. In this case, N-Q sites were only influenced by chloride ions (Cl^-) in acidic region and hydroxy ions (OH^-) in basic region. On the other hand, the surface of Z6 might be occupied with other nitrogen species (N-5, N-6) and/or $\text{C}\pi$ sites which is always influenced by solution

pH leading to the wide range of surface proton (H^+) concentrations from acidic (higher proton concentration) to basic region (lower proton concentration).

Activated carbon fiber (ACF) is a useful carbon material from the point of handling. Nitrogen doping into ACF was conducted by thermal chemical vapor deposition (CVD) by charging acetonitrile (CH_3CN) into ACF [53]. Rayon-based ACF (Toyobo Co., Ltd.), namely, KF1500, was employed as a starting material. KF1500 is microporous ACF produced as a commercial product from cellulose (rayon polymer), and it has average pore diameter (D_{avg}) of 1.8 nm and specific surface area (S_{BET}) of 1,540 m^2/g . In our study at first KF1500 was further activated with super heat steam at 800°C to expand pore volume by sending pure water to quartz tube readily heated in a tube furnace at the desired temperature in which KF1500 sample (2–3 g) was placed on a boat. In the next step, the flow of steam was switched to the acetonitrile liquid under inert gas flow, and nitrogen deposition with thermal CVD started, and nitrogen was continuously doped inside KF1500 accompanied by plugging the pore structure with carbonization of acetonitrile. Since the resultant KF1500 must have contained more than 4% nitrogen but very small specific surface area around 10 m^2/g , post-heat treatment at 950°C and steam activation at 800°C were carried out to raise the N-Q content by converting N-6 in doped nitrogen to N-Q [51] and increase specific surface area [54], respectively. Figure 18 shows nitrate adsorption onto modified KF1500 ACFs compared with those derived from phenol resin referred to as PhR (Kynol, Gun Ei Chemical Industry Co., Ltd.) [53]. The pristine material of KF1500 adsorbs nitrate by 0.36 mmol/g, and it contains 0.33% of quaternary nitrogen (N-Q) because some nitrogen compounds were mixed with rayon resin in the process of manufacturing KF1500. The further steam activation of KF1500 at 800°C (KF-8ST30) in our laboratory resulted in the increase in adsorption amount of nitrate from 0.36 to 0.55 mmol/g by expanding specific surface area from 1,560 to 1960 m^2/g , but no

Fig. 18 Adsorption amount of nitrate on ACFs derived from phenol resin (PhR) and ACFs modified of KF1500 (KF) and corresponding quaternary nitrogen content (N-Q, filled diamond) in ACFs. 8ST10; steam activation at 800°C by charging 10 mL water, 9.5HT30; heat treated at 950°C for 30 min, 8AN20; thermal CVD at 800°C by charging 20 mL of acetonitrile. Initial nitrate concentration of 200 mg- NO_3^-/L , equilibrium solution pH (pH_e) 3.0 [53]



N-Q was detected. Thereby the increase in nitrate adsorption is attributed to not N-Q content but $C\pi$ sites increased by enlarging graphene sheets exposed. While just heat treatment of KF1500 (KF-9.5HT30) makes the adsorption amount increase up to 0.52 mmol/g, only nitrogen doping with acetonitrile into KF1500 (KF-8AN20) could not improve nitrate adsorption even though N-Q content is increased as great as 1.95%. This is caused by plugging of pore during nitrogen doping with acetonitrile at 800°C supported by the fact that only 10 m²/g of specific surface area could be measured for KF-8AN20. Then several combinations of steam activation at 800°C (8ST), nitrogen doping with acetonitrile at 800°C (8AN), and heat treatment to form N-Q at 950°C (9.5HT) were attempted, and the order of steam activation, nitrogen doping, heat treatment, and steam activation again (KF-8ST10-8AN20-9.5HT30-8ST30) was found to be the optimum for nitrate adsorption of 0.74 mmol/g among all combinations examined in the study. At the same time N-Q content is 1.86% next to 1.95% of KF-8AN20, although specific surface area is a little declined from 1,540 m²/g (KF1500) to 1,360 m²/g (KF-8ST10-8AN20-9.5HT30-8ST30). On the other hand, for phenol resins (PhRs) similar treatments without nitrogen doping (PhR-8ST10-9.5HT30-8ST30) were conducted, and no N-Q was detected and adsorption amount of nitrate attained 0.49 mmol/g. Similar treatments also applied to KF1500 (KF-8ST10-9.5HT30-8ST30) and similar results with PhR were obtained for nitrate uptake. The above results imply that nitrogen doping at 800°C followed by heat treatment at 950°C and finally steam activation may be one of the best procedures to maximize both specific surface area and N-Q contents exposed on ACF surface. Figure 19 represents XPS N1s signals of pristine KF1500 and nitrogen-doped KF1500 (KF-8ST10-8AN20-95HT30-8ST30) [53]. When trimethylammonium (quaternary amino groups, a kind of N-Q)-functionalized ion-exchange resin was used for nitrate adsorption, adsorption amount of nitrate was constant for a wide range of equilibrium solution pH as shown in Fig. 20 [55]

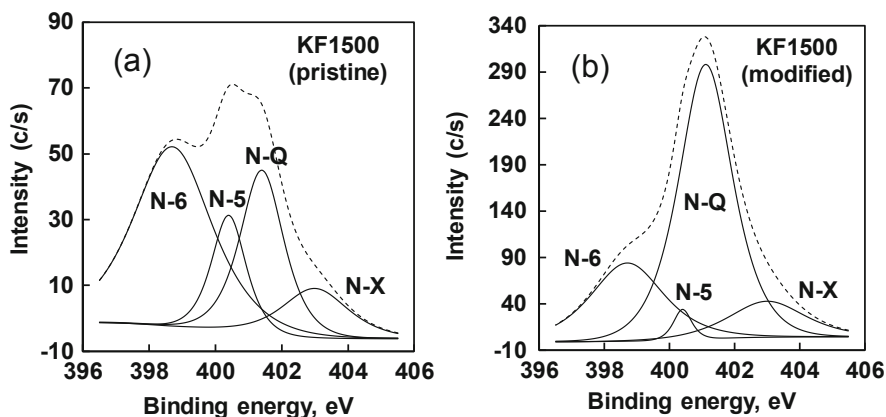


Fig. 19 XPS N1s spectra and deconvolution results of KF1500 (pristine (a) and modified (b)). Modified conditions; steam activation at 800°C by 10 mL water, nitrogen thermal CVD doping at 800°C with 20 mL acetonitrile solvent, heat treatment at 950°C in inert gas for 30 min, and steam activation at 800°C by 30 mL water again (KF-8ST10-8AN20-95HT30-8ST30) [53]

Fig. 20 Influence of equilibrium solution pH (pH_e) on nitrate adsorption onto trimethylammonium (quaternary amino groups)-functionalized ion exchange resin (HP555). Initial nitrate concentration of 200 mg- NO_3^-/L [55]

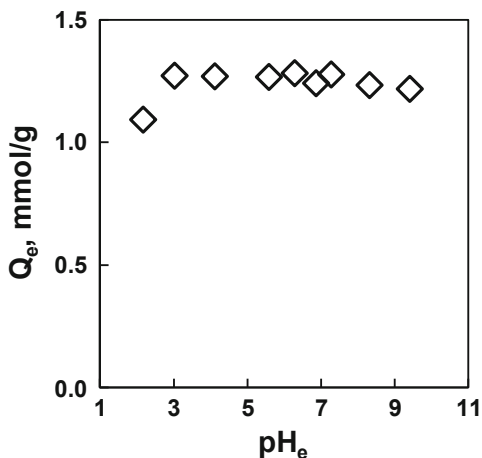
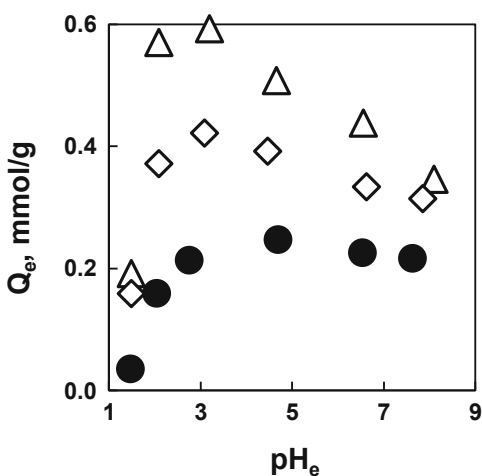


Fig. 21 Influence of equilibrium solution pH (pH_e) on nitrate adsorption onto modified KF1500 (KF-8ST10-8AN20-9.5HT30-8ST10). Initial nitrate concentration of 200 mg- NO_3^-/L (open triangle), 100 mg/L (open diamond), and 40 mg/L (filled circle) at ambient temperature [56]



indicating that N-Q could adsorb nitrate independent on solution pH due to positively charged nitrogen of N-Q ($\text{R-N}^+(\text{CH}_3)_3\text{Cl}^-$) which strongly attracted nitrate anion. N-Q composition and content of the nitrogen-doped KF1500 compared with N-6 are much greater than the pristine KF1500. Based on the results, specific surface area and N-Q content are estimated to play an important role for the nitrate adsorption. To inspect the hypothesis, influence of solution pH on the adsorption of nitrate onto the nitrogen-doped KF1500 was inspected using various initial concentrations of nitrate as displayed in Fig. 21 [56]. In the figure, the number of variations of initial concentrations of nitrate was limited to 3, but we can explain the adsorption sites of the nitrogen-doped KF1500. As long as we understand considering our previous study, $\text{C}\pi$ sites are strongly influenced by solution pH; when solution pH is adjusted with HCl and NaOH, in acidic region protons (H^+) are concentrated on $\text{C}\pi$ sites, and the positively charged graphene attracts nitrate anion, but much amount of Cl^- anion

(strong HCl acid) hinders the approach of nitrate (NO_3^-) onto the positive surface charge with competitive adsorption between Cl^- and NO_3^- . In NaOH basic region, OH^- is competitive with NO_3^- , and graphene layer itself becomes negative charge causing the decline of nitrate adsorption. As can be seen in Fig. 21, equilibrium adsorption amount of nitrate (Q_e) exhibits the maximum value (0.59 mmol/g) at pH 3 and gradually decreased toward 0.3 mmol/g at pH 5 to 8 in case of the initial nitrate concentration of 200 mg/L. Similar tendency was observed for the initial nitrate concentration of 100 mg/L, but nearly constant amounts could be seen for 40 mg/L. The results reveal that there are strong adsorption sites that can be always positively charged in changing solution pH and weak adsorption sites that are easily influenced by solution pH; the former should be N-Q sites, and the latter can be $\text{C}\pi$ sites. When the total adsorption amount is about 0.6 mmol/g, a part of it can be attributed to $\text{C}\pi$ sites (0.3 mmol/g); the other part will be come from N-Q sites (0.3 mmol/g).

Polyacrylonitrile (PAN) fiber is one of the promising materials to prepare nitrogen-containing adsorbents because it contains 20% nitrogen in the PAN structure at the flame-resistant forms [57]. White colored polymer of polyacrylonitrile (PAN) resin is at first carefully treated in air to stabilize the PAN resin [58–60]; otherwise, PAN fiber will be easily turned to carbon cake without remaining fiber morphology in the post-activation process at 500°C or more. In the first stage, we prepared the flame-resistant PAN fiber to optimize air treatment conditions [60], but commercially available black colored insolubilized PAN fiber, namely, PYROMEX was purchased from Teijin Co., Ltd. (former Toho Tenax Co., Ltd.), to accelerate the examination of post-activation treatments. Since PYROMEX fiber is supplied as a felt shaped material, we can easily handle PYROMEX for the various treatments. At first, PYROMEX (hereafter designated as PYR) was activated with steam at 800°C to improve the porous structure. Three grams of PYR were placed in a quartz tube and heated up to 800°C, and then 20 mL pure water was charged into quartz tube to develop porous structure in PYR with super-heated steam (PYR-8ST20). PYR-8ST20 was further treated at 950°C in inert gas to convert N-6 to N-Q species [51]. For the comparison, cellulose-based KF1500 was heat-treated at 950°C as well. Figure 22 displays the SEM images of the materials revealing that original morphology can be maintained after the steam and heat treatments. In Table 3 were shown properties of the prepared samples [57]. Specific surface area of PYR went up from 9 m²/g to 790 m²/g (PYR-8ST20) by the steam activation, whereas nitrogen content significantly declined from 20.9% to 5.6%. Post-treatment of PYR-8ST20 at 950°C for 30 min (PYR-8ST20-9.5HT30) resulted in the decline of specific surface area and nitrogen and oxygen content. N-Q content was also decreased from 0.56% to 0.51%, but adsorption amount of nitrate went up from 0.47 mmol/g (PYR-8ST20) to 0.64 mmol/g (PYR-8ST20-9.5HT30) [57]. The increase in adsorption amount of nitrate can be attributed to not only N-Q content but also lower oxygen content, because oxygen including acidic functional groups on carbon surface can inhibit nitrate adsorption [57]. KF1500-9.5HT30 was used as a reference material because heat treatment at 950°C could reduce acidic oxygen functional groups. Resultant oxygen content was 10.6% close to the value of PYR-8ST20-9.5HT30 (9.3%), and it has twice larger specific surface area but less N-Q content than PYR-8ST20-

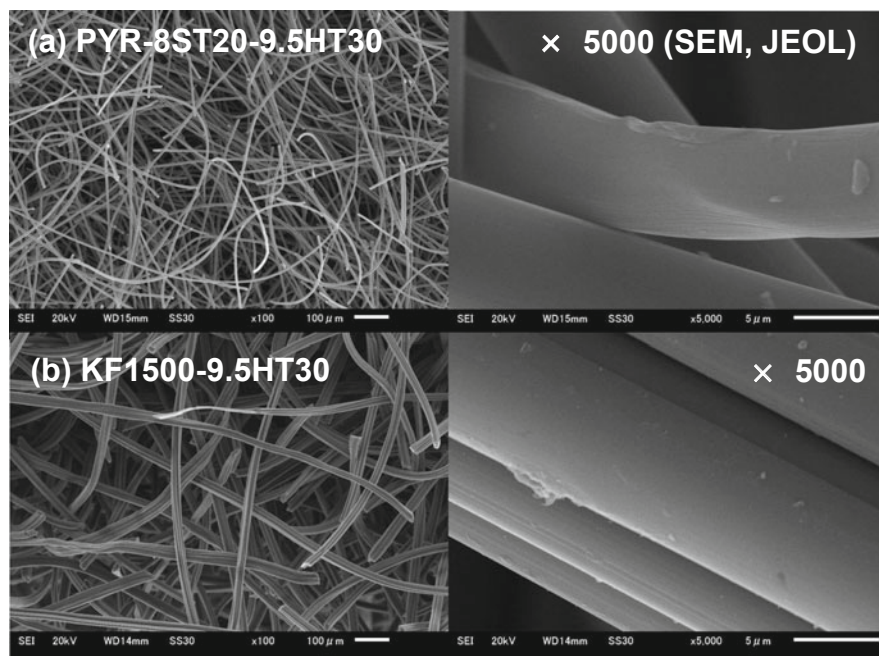


Fig. 22 SEM image of PAN-based ACF (a) (upper pictures, PYR-8ST20-9.5HT30) and cellulose-based ACF (b) (lower pictures, KF1500-9.5HT30) as a reference material using scanning electron microscope (JEOL JSM-6510) [57]

9.5HT30. Figure 23 shows the adsorption of nitrate as a function of equilibrium solution pH (pH_e) at the initial nitrate concentration of 50 mg/L (a) and 200 mg/L (b) [57]. PYR-8ST20-9.5HT30 is always better than KF1500-9.5HT30 at any condition; however, maximum points can be observed at the initial nitrate concentration of 50 mg/L for the both adsorbents, but not at 200 mg/L. In the lower nitrate concentration, adsorption amount is easily influenced by co-existing anions as chloride (Cl^-) and hydroxide (OH^-) in acidic and basic regions, respectively. Furthermore, decreasing slopes toward neutral region are more pronounced for PYR-8ST20-9.5HT30 than KF1500-9.5HT30 indicating that pH-insensitive N-Q sites are dominant for PYR-8ST20-9.5HT30, whereas pH-sensitive $\text{C}\pi$ sites are predominant for KF1500-9.5HT30 as well.

Other than nitrate, anionic contaminant of phosphate can be removed with the PYR adsorbents. In our experiences, adsorbents suitable to nitrate cannot be directly applied to the capture of phosphate, although phosphate is also present in aqueous phase as negatively charged anions in a wide range of solution pH above 2 (non-ionic H_3PO_4 species at solution pH less than 2). In case of PAN ACF (PYROMEX), activation with K_2CO_3 may be the best procedure for the preparation of adsorbent to remove phosphate. The original fiber morphology is not changed even though the chemical activation with K_2CO_3 is employed. When other chemicals such as ZnCl_2 , H_3PO_4 , and KOH were used for activation, fiber morphology was broken from the pristine PYROMEX status. The K_2CO_3 activation was conducted at 800°C in the

Table 3 Properties of PAN-based and cellulose-based activated carbon fibers (ACFs) activated by steam and annealed [57]

Sample name	Textural and surface properties				Elemental composition				Nitrogen configuration				
	S_{BET} , m^2/g	Pore volume (V_{total}), cm^3/g	Micropore volume (V_{micro}), cm^3/g	Mesopore volume (V_{meso}), cm^3/g	pH_{pzc}	Carbon, %	Hydrogen, %	Nitrogen, %	Oxygen, %	Pyridine (N-6), %	Pyrrole (N-5), %	Quaternary (N-Q), %	Pyridine- N-oxide, etc. (N-X), %
PYROMEX	9	0.004	0.003	0.001	-	59.6	3.6	20.9	15.9	-	-	-	-
PYR-8ST20	790	0.34	0.33	0.01	-	73.0	0.8	5.6	20.6	2.60	0.86	0.56	1.58
PYR-8ST20- 9.5HT30	710	0.32	0.32	0.005	5.3	86.7	0.5	3.6	9.3	0.92	0.36	0.51	1.78
KFI500- 9.5HT30	1,530	0.68	0.66	0.03	5.4	87.4	0.3	1.7	10.6	0.65	0.25	0.28	0.51

^aCalculated by difference

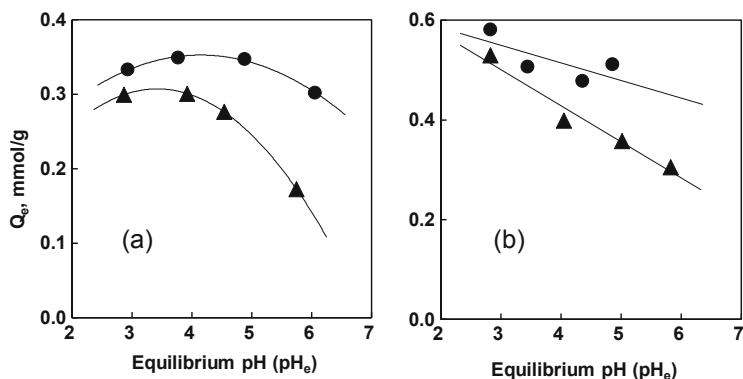


Fig. 23 Influence of equilibrium solution pH (pH_e) on the amount of nitrate adsorption onto PYR-8ST20-9.5HT30 (filled circle) and KF1500-9.5HT30 (filled triangle) at the initial nitrate concentrations of 50 mg-NO₃⁻/L (a) and 200 mg-NO₃⁻/L (b). Adsorption conditions; 30 mg adsorbent dosage into 15 mL nitrate solution [57]

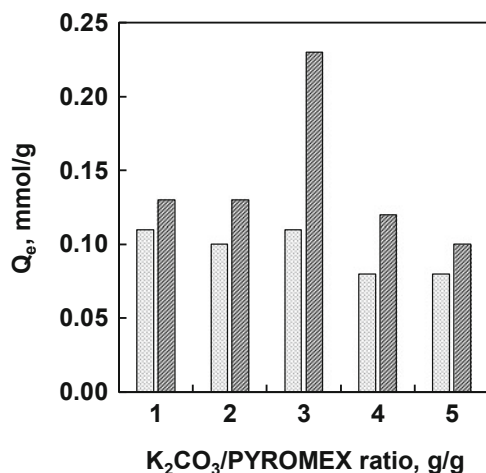


Fig. 24 Equilibrium adsorption amount of phosphate (Q_e) on PYR-KC1 (or 2, 3, 4, 5) (light bar) and PYR-KC1 (or 2, 3, 4, 5)-9.5HT30 (dark bar). Initial KH₂PO₄ concentration; 3 mmol/L, adsorbent dosage; 2 g/L [61]

impregnation ratio of K₂CO₃/PYROMEX ranging 1–5 by step 1, referred to as PYR-KC3 in case of the impregnation ratio of 3. Post-heat treatment at 950°C for 30 min was carried out for PYR-KC1 (and 2, 3, 4, 5) to obtain PYR-KC1 (and 2, 3, 4, 5)-9.5HT30 as well. Figure 24 displays the adsorption of phosphate on the ten prepared samples from PYROMEX [61]. All heat treatment samples captured greater amount of phosphate than all corresponding samples before the heat treatment. In the PYR-KC-9.5HT30 series, PYR-KC3-9.5HT30 exhibited exceptionally better adsorption performance than the other PYR-KC-9.5HT30 series. Table 4

Table 4 Textural, bulk and surface properties of ACFs derived from PYROMEX using K_2CO_3 activation and annealing [61]

Sample from PYROMEX	Textural analysis		Elemental analysis, wt%				XPS analysis, wt%			
	S_{BET} , m^2/g	V_{total} , cm^3/g	Carbon	Hydrogen	Nitrogen	Oxygen ^a	N-6	N-5	N-Q	N-X
PYR-KC1	2,040	0.998	74.8	0.5	6.7	18.0	-	-	-	-
PYR-KC3	1,720	0.807	89.4	<0.1	0.9	9.6	0.14	0.49	0.33	0.11
PYR-KC5	1,800	0.675	89.1	<0.1	0.6	10.2	-	-	-	-
PYR-KC1-9.5HT30	870	0.411	87.9	<0.1	1.3	10.7	0.19	0.19	0.50	0.30
PYR-KC3-9.5HT30	1,280	0.559	90.0	<0.1	1.2	8.7	0.30	0.40	0.46	0.19
PYR-KC5-9.5HT30	1,940	0.911	85.6	<0.1	0.5	13.8	0.05	0.24	0.25	0.20

^aCalculated by difference

shows textural and surface properties of the ten samples prepared from PYROMEX using K_2CO_3 activation [61]. For PYR-KC series, lower N-Q and higher oxygen content (oxygen functional groups) might reduce the adsorption amounts of phosphate compared to PYR-KC-9.5HT30 series. After the heat treatment, oxygen-containing functional groups must have been removed, and N-Q content was increased. PYR-KC3-9.5HT30 is better than PYR-KC1-9.5HT30 because pore structure has not been sufficiently developed although N-Q in PYR-KC1-9.5HT30 (0.50 wt%) is slightly larger than PYR-KC3-9.5HT30 (0.46 wt%); effective adsorption sites of N-Q might not be exposed to phosphate anion due to lower specific surface area. On the other hand, even though PYR-KC5-9.5HT30 has larger specific surface area than PYR-KC3-9.5HT30, adsorption amount of phosphate of the latter is greater than the former. This is caused by significant decrease in N-Q content of PYR-KC5-9.5HT30 (0.25 wt%) compared with PYR-KC3-9.5HT30 (N-Q, 0.46 wt%). Consequently PYR-KC3-9.5HT30 is the optimum adsorbent for phosphate removal under the balance of N-Q and oxygen content and specific surface area including the extent of exposure of N-Q on the carbon surface.

Nitrogen-doped ACs and ACFs can be derived from numerous materials and procedures; thereby, we believe that there are still much room to develop more excellent materials to capture anionic contaminants such as bean dregs (by-product in the production of bean cake that is “TOFU” in Japanese) that contains nitrogen by 4.6 wt% in dry base [62] and bamboo activated with $ZnCl_2$ followed by ammonia (NH_3) gas treatment at $950^\circ C$ [63]. Nitrogen doping with thermal CVD treatment of ACF by aniline in place of acetonitrile was effective for arsenic ($As(V)$; $HAsO_4^{2-}$, AsO_4^{3-}) adsorption as well [64, 65]. Hexavalent chromium ($Cr(VI)$) is dissolved in aqueous phase as anions such as $Cr_2O_7^{2-}$, CrO_4^{2-} , and $HCrO_4^-$ [66]. These $Cr(VI)$ species can be captured with above N-doped materials [62, 63].

4 Conclusion

Modification of activated carbon is effective for improving adsorption affinity and capacity of organic and inorganic pollutants in water. Small and large molecules, e.g., mono-aromatics and tannic acids, respectively, are included as organic molecules. Heavy metals of cations (Cd^{2+} , Pb^{2+} , Ni^{2+} , etc.) and anions (NO_3^- , $H_2PO_4^-$, $HAsO_4^{2-}$, $Cr_2O_7^{2-}$, etc.) are involved in inorganic pollutants. For adsorptive removal of organic contaminants, high specific surface area sometimes with meso- and macropore and less oxygen content are preferable for ACs and ACFs. To capture cationic heavy metals, carboxy, sulfonic, and thiol groups ACs and ACFs are effective on, although only sulfonic function has not been sufficiently formed yet on carbon surface. For the adsorptive removal of anionic contaminants, nitrogen functional groups such as quaternary nitrogen (N-Q) and alkyl amine and less oxygen groups may be essential to effective uptake of anions. N-Q functional ACs and ACFs are now under development, but binding alkyl amine onto carbon surface has still been challenging subject.

Acknowledgments This review study was supported in part Grants-in-Aid for Scientific Research (C) from the Japan Society for the Promotion of Science (KAKENHI Grant No. JP20K05187). Prof. Dr. Fumio Imazeki, the head of Safety and Health Organization, Chiba University, is sincerely acknowledged for his encouragement and the financial support of our study. Gratitude is greatly extended to Ms. Shizuka Ishibashi, Safety and Health Organization, Chiba University, for her dedicated support in preparing the review manuscripts.

References

1. Konstantinou IK, Hela DG, Albanis TA (2006) The status of pesticide pollution in surface waters (rivers and lakes) of Greece. Part I. review on occurrence and levels. *Environ Pollut* 141 (3):555–570. <https://doi.org/10.1016/j.envpol.2005.07.024>
2. Jones OAH, Voulvoulis N, Lester JN (2004) Potential ecological and human health risks associated with the presence of pharmaceutically active compounds in the aquatic environment. *Crit Rev Toxicol* 34(4):335–350. <https://doi.org/10.1080/10408440490464697>
3. Kleywegt S, Pileggi V, Yang P, Hao C, Zhao X, Rocks C, Thach S, Cheung P, Whitehead B (2011) Pharmaceuticals, hormones and bisphenol A in untreated source and finished drinking water in Ontario, Canada — occurrence and treatment efficiency. *Sci Total Environ* 409 (8):1481–1488. <https://doi.org/10.1016/j.scitotenv.2011.01.010>
4. Pan K, Wang W-X (2012) Trace metal contamination in estuarine and coastal environments in China. *Sci Total Environ* 421-422:3–16. <https://doi.org/10.1016/j.scitotenv.2011.03.013>
5. Wang S-L, Xu X-R, Sun Y-X, Liu J-L, Li H-B (2013) Heavy metal pollution in coastal areas of South China: a review. *Mar Pollut Bull* 76(1–2):7–15. <https://doi.org/10.1016/j.marpolbul.2013.08.025>
6. Li Z, Ma Z, van der Kuijp TJ, Yuan Z, Huang L (2014) A review of soil heavy metal pollution from mines in China: pollution and health risk assessment. *Sci Total Environ* 468-469:843–853. <https://doi.org/10.1016/j.scitotenv.2013.08.090>
7. Yang Q, Li Z, Lu X, Duan Q, Huang L, Bi J (2018) A review of soil heavy metal pollution from industrial and agricultural regions in China: pollution and risk assessment. *Sci Total Environ* 642:690–700. <https://doi.org/10.1016/j.scitotenv.2018.06.068>
8. Wei B, Yang L (2010) A review of heavy metal contaminations in urban soils, urban road dusts and agricultural soils from China. *Microchem J* 94(2):99–107. <https://doi.org/10.1016/j.microc.2009.09.014>
9. Qin B, Zhou J, Elser JJ, Gardner WS, Deng J, Brookes JD (2020) Water depth underpins the relative roles and fates of nitrogen and phosphorus in lakes. *Environ Sci Technol* 54:3191–3198. <https://doi.org/10.1021/acs.est.9b05858>
10. Kraal P, Burton ED, Rose AL, Cheetham MD, Bush RT, Sullivan LA (2013) Decoupling between water column oxygenation and benthic phosphate dynamics in a shallow eutrophic estuary. *Environ Sci Technol* 47(7):3114–3121. <https://doi.org/10.1021/es304868t>
11. Sprague LA, Hirsch RM, Aulenbach BT (2011) Nitrate in the Mississippi river and its tributaries, 1980 to 2008: are we making progress? *Environ Sci Technol* 45(17):7209–7216. <https://doi.org/10.1021/es201221s>
12. Burow KR, Nolan BT, Rupert MG, Dubrovsky NM (2010) Nitrate in groundwater of the United States, 1991-2003. *Environ Sci Technol* 44(13):4988–4997. <https://doi.org/10.1021/es100546y>
13. Leone A, Ripa MN, Uricchio V, Deák J, Vargay Z (2009) Vulnerability and risk evaluation of agricultural nitrogen pollution for Hungary's main aquifer using DRASTIC and GLEAMS models. *J Environ Manag* 90(10):2969–2978. <https://doi.org/10.1016/j.jenvman.2007.08.009>
14. Liu GD, Wu WL, Zhang J (2005) Regional differentiation of non-point source pollution of agriculture-derived nitrate nitrogen in groundwater in northern China. *Agric Ecosyst Environ* 107(2–3):211–220. <https://doi.org/10.1016/j.agee.2004.11.010>

15. Wang J, Guo X (2020) Adsorption kinetic models: Physical meanings, applications, and solving methods. *J Hazard Mater* 390:122156. <https://doi.org/10.1016/j.jhazmat.2020.122156>
16. Hubbe MA, Azizian S, Douven S (2019) Implications of apparent pseudo-second-order adsorption kinetics onto cellulosic materials: a review. *Bio Res* 14(3):7582–7626
17. Fan S, Wang Y, Wang Z, Ji T, Tang J, Li X (2017) Removal of methylene blue from aqueous solution by sewage sludge-derived biochar: adsorption kinetics, equilibrium, thermodynamics and mechanism. *J Environ Chem Eng* 5:601–611. <https://doi.org/10.1016/j.jece.2016.12.019>
18. Wu F-C, Tseng R-L, Juang R-S (2001) Kinetic modeling of liquid-phase adsorption of reactive dyes and metal ions on chitosan. *Water Res* 35(3):613–618. [https://doi.org/10.1016/S0043-1354\(00\)00307-9](https://doi.org/10.1016/S0043-1354(00)00307-9)
19. Bhattacharyya KG, Sharma A (2005) Kinetics and thermodynamics of Methylene Blue adsorption on Neem (*Azadirachta indica*) leaf powder. *Dyes Pigments* 65:51–59. <https://doi.org/10.1016/j.dyepig.2004.06.016>
20. Oishi S, Amano Y, Aikawa M, Machida M (2011) Adsorption of Pb(II) ion on mesoporous activated carbon prepared by ZnCl₂ activation. *TANSO* 2011(250):231–237. <https://doi.org/10.7209/tanso.2011.231>
21. Goto T, Amano Y, Machida M, Imazeki F (2015) Effect of polarity of activated carbon surface, solvent and Adsorbate on adsorption of aromatic compounds from liquid phase. *Chem Pharm Bull* 63(9):726–730. <https://doi.org/10.1248/cpb.c15-00039>
22. Ramis G, Busca G, Lorenzelli V (1993) Determination of the geometry of adsorbed unsaturated molecules through the analysis of the CH out-of-plane deformation modes. *J Electron Spectrosc Relat Phenom* 64–65:297–305. [https://doi.org/10.1016/0368-2048\(93\)80091-Y](https://doi.org/10.1016/0368-2048(93)80091-Y)
23. Chen L, Tanner EEL, Richard G, Compton RG (2017) Adsorption on graphene: flat to edge to end transitions of phenyl hydroquinone. Adsorption on graphene: flat to edge to end transitions of phenyl hydroquinone. *Phys Chem Chem Phys* 19:17521–17525. <https://doi.org/10.1039/c7cp03261g>
24. Sakazaki T, Oishi S, Amano Y, Machida M (2011) Adsorption properties of large molecule on activated carbons prepared from Urame oak and coconut shell char. *Kagaku Kogaku Ronbunshu* 37(5):381–387. <https://doi.org/10.1252/kakoronbunshu.37.381>
25. Tamon H, Okazaki M (1996) Desorption characteristics of aromatic compounds in aqueous solution on solid adsorbents. *J Colloid Interface Sci* 179(1):181–187. <https://doi.org/10.1006/jcis.1996.0200>
26. Machida M, Amano Y, Imazeki F (2015) Water purification with activated carbons (ACs): a short review - influence of the textural and surface properties of ACs on the adsorptive removal of pollutants. *Carbon* 2015(270):241–249. <https://doi.org/10.7209/tanso.2015.241>
27. Harris PJF, Tsang SC (1997) High-resolution electron microscopy studies of non-graphitizing carbons. *Philos Mag A* 76(3):667–677. <https://doi.org/10.1080/01418619708214028>
28. Huang J-JS, Lin S-C, Lowemark L, Liou SYH, Chang Q, Chang T-K, Wei K-Y, Croudace IW (2019) Rapid assessment of heavy metal pollution using ion-exchange resin sachets and micro-XRF core-scanning. *Sci Rep* 9(1):1–6. <https://doi.org/10.1038/s41598-019-43015-x>
29. Ming Hua M, Shujuan Zhang S, Bingcai Pan B, Weiming Zhang W, Lu Lv L, Quanxing Zhang Q (2012) Heavy metal removal from water/wastewater by nanosized metal oxides: a review. *J Hazard Mater* 211–212:317–331. <https://doi.org/10.1016/j.jhazmat.2011.10.016>
30. Machida M, Amano Y (2020) Development of carbonaceous porous adsorbents to remove ionic pollutants from aqueous solution. *Shokubai* 62(3):190–196. <https://cats.jp/jnl/pageview?articlecd=62030010000>
31. Moreno-Castilla C, Ferro-Garcia MA, Joly JP, Bautista-Toledo I, Carrasco-Marin F, Rivera-Utrilla J (1995) Activated carbon surface modifications by nitric acid, hydrogen peroxide, and ammonium peroxydisulfate treatments. *Langmuir* 11:4386–4392. <https://doi.org/10.1021/la00011a035>
32. Nemoto Y, Iitsuka Y, Watanabe K, Amano Y, Machida M (2016) Adsorptive removal of Ni (II) from water using oxidized activated carbon derived from sulfur containing petroleum coke. *Kagaku Kogaku Ronbunshu* 42(4):142–147. <https://doi.org/10.1252/kakoronbunshu.42.142>

33. Sato K, Izza A, Watanabe K, Hagiwara K, Kato M, Amano Y, Machida M (2019) Preparation of sulfur-contained activated carbon from petroleum coke. *J Jpn Pet Inst* 62(5):205–210. <https://doi.org/10.1627/jpi.62.205>
34. Kim D, Jung YW, Kwon S, Park J-W (2011) Adsorption of cadmium(II) from aqueous solutions by thiol-functionalized activated carbon. *Water Sci Technol Water Supply* 11(1):61–66. <https://doi.org/10.2166/ws.2011.009>
35. Machida M, Fotoohi B, Amano Y, Mercier L (2012) Cadmium(II) and lead(II) adsorption onto hetero-atom functional mesoporous silica and activated carbon. *Appl Surf Sci* 258:7389–7394. <https://doi.org/10.1016/j.apsusc.2012.04.042>
36. Sato S, Yoshihara K, Moriyama K, Machida M, Tatsumoto H (2007) Influence of activated carbon surface acidity on adsorption of heavy metal ions and aromatics from aqueous solution. *Appl Surf Sci* 253:8554–8559. <https://doi.org/10.1016/j.apsusc.2007.04.025>
37. Machida M, Mochimaru T, Tatsumoto H (2006) Lead(II) adsorption onto the graphene layer of carbonaceous materials in aqueous solution. *Carbon* 44(13):2681–2688. <https://doi.org/10.1016/j.carbon.2006.04.003>
38. Machida M, Chensun S, Amano Y, Imazeki F (2015) Adsorptive removal of Pb(II) ions from aqueous solution by (NH₄)₂S₂O₈ oxidized activated carbon. *Bull Chem Soc Jpn* 88:127–132. <https://doi.org/10.1246/bcsj.20140124>
39. Mena Aguilar KM, Amano Y, Machida M (2016) Ammonium persulfate oxidized activated carbon fiber as a high capacity adsorbent for aqueous Pb(II). *J Environ Chem Eng* 4:4644–4652. <https://doi.org/10.1016/j.jece.2016.10.028>
40. Li N, Ma X, Zha Q, Kim K, Chen Y, Song C (2011) Maximizing the number of oxygen-containing functional groups on activated carbon by using ammonium persulfate and improving the temperature-programmed desorption characterization of carbon surface chemistry. *Carbon* 49:5002–5013. <https://doi.org/10.1016/j.carbon.2011.07.015>
41. Weast RC (1994) *Handbook of chemistry and physics*. 75th edn. CRC Press, Boca Raton, pp D159–D161
42. Bitter JH, van Dommele S, de Jong KP (2010) On the virtue of acid-base titrations for the determination of basic sites in nitrogen doped carbon nanotubes. *Catal Today* 150:61–66. <https://doi.org/10.1016/j.cattod.2009.09.008>
43. Dioum A, Hamoudi S (2014) Mono- and quaternary-ammonium functionalized mesoporous silica materials for nitrate adsorptive removal from water and wastewaters. *J Porous Mater* 21:685–690. <https://doi.org/10.1007/s10934-014-9815-6>
44. Ota K, Amano Y, Aikawa M, Machida M (2012) Removal of nitrate ions from water by activated carbons (ACs) - influence of surface chemistry of ACs and coexisting chloride and sulfate ions. *Appl Surf Sci* 276:838–842. <https://doi.org/10.1016/j.apsusc.2013.03.053>
45. Figueiredo JL, Pereira MFR, Freitas MMA, Órfão JJM (1999) Modification of the surface chemistry of activated carbons. *Carbon* 37(9):1379–1389. [https://doi.org/10.1016/S0008-6223\(98\)00333-9](https://doi.org/10.1016/S0008-6223(98)00333-9)
46. Iida T, Amano Y, Aikawa M, Machida M (2013) The effect of the surface property of activated carbon on nitrate adsorption. *Kankyo Kagaku* 23(2):91–94. <https://doi.org/10.5985/jec.23.91>
47. Machida M, Fotoohi B, Amano Y, Mercier L (2012) Cadmium(II) and lead(II) adsorption onto hetero-atom functional mesoporous silica and activated carbon. *Appl Surf Sci* 258:7389–7394. <https://doi.org/10.1016/j.apsusc.2012.04.042>
48. Machida M, Fotoohi B, Amano Y, Ohba T, Kanoh H, Mercier L (2012) Cadmium (II) adsorption using functional mesoporous silica and activated carbon. *J Hazard Mater* 221-222:220–227. <https://doi.org/10.1016/j.jhazmat.2012.04.039>
49. Byrne TM, Gu X, Hou P, Cannon FS, Brown NR, Nieto-Delgado C (2014) Quaternary nitrogen activated carbons for removal of perchlorate with electrochemical regeneration. *Carbon* 73:1–12. <https://doi.org/10.1016/j.carbon.2014.02.020>
50. Machida M, Goto T, Amano Y, Iida T (2016) Adsorptive removal of nitrate from aqueous solution using nitrogen doped activated carbon. *Chem Pharm Bull* 64:1555–1559. <https://doi.org/10.1248/cpb.c16-00368>

51. Pels JR, Kapteijn F, Moulijn JA, Zhu Q, Thomas KM (1995) Evolution of nitrogen functionalities in carbonaceous materials during pyrolysis. *Carbon* 33(11):1641–1653. [https://doi.org/10.1016/0008-6223\(95\)00154-6](https://doi.org/10.1016/0008-6223(95)00154-6)
52. Goto T, Amano Y, Machida M (2017) Surface modification of carbonized melamine sponge by methyl iodide for the efficient removal of nitrate ions. *Tanso* 2017(276):2–7. <https://doi.org/10.7209/tanso.2017.2>
53. Yuan J, Amano Y, Machida M (2019) Surface modified mechanism of activated carbon fibers by thermal chemical vapor deposition and nitrate adsorption characteristics in aqueous solution. *Colloids Surf A Physicochem Eng Asp* 580:123710. <https://doi.org/10.1016/j.colsurfa.2019.123710>
54. Machida M, Yoo P, Amano Y (2019) Adsorption of nitrate from aqueous phase onto nitrogen-doped activated carbon fibers (ACFs). *SN Appl Sci* 1(4):1–7. <https://doi.org/10.1007/s42452-019-0333-7>
55. Kino K, Sakamoto T, Yuan J, Amano Y (2020) Quaternary nitrogen functionalized carbonaceous adsorbents to remove nitrate from aqueous phase. *Catal Today*. <https://doi.org/10.1016/j.cattod.2020.06.036>
56. Yuan J, Amano Y, Machida M (2019) Study on the characteristics of nitrogen-doped activated carbon fibers to remove nitrate ions by multi-factor analysis. *Int J Environ Sci Technol* 17(5):2563–2570. <https://doi.org/10.1007/s13762-020-02663-7>
57. Machida M, Sakamoto T, Sato K, Goto T, Amano Y (2018) Adsorptive removal of nitrate from aqueous phase using steam activated and thermal treated polyacrylonitrile (PAN) fiber. *J Fiber Sci Technol* 74(7):158–164. <https://doi.org/10.2115/fiberst.2018-0023>
58. Surianarayanan M, Vijayaraghavan R, Raghavan KV (1998) Spectroscopic investigations of polyacrylonitrile thermal degradation. *J Polym Sci Part A Polym Chem* 36(14):2503–2512. [https://doi.org/10.1002/\(SICI\)1099518\(199810\)36:14<2503::AID-POLA9>3.0.CO;2-T](https://doi.org/10.1002/(SICI)1099518(199810)36:14<2503::AID-POLA9>3.0.CO;2-T)
59. Dalton S, Heatley F, Budd PM (1999) Thermal stabilization of polyacrylonitrile fibers. *Polymer* 40(20):5531–5543. [https://doi.org/10.1016/S0032-3861\(98\)00778-2](https://doi.org/10.1016/S0032-3861(98)00778-2)
60. Zaini MAA, Amano Y, Machida M (2010) Adsorption of heavy metals onto activated carbons derived from polyacrylonitrile fiber. *J Hazard Mater* 180(1–3):552–560. <https://doi.org/10.1016/j.jhazmat.2010.04.069>
61. Sakamoto T, Amano Y, Machida M (2020) Phosphate ion adsorption properties of PAN-based activated carbon fibers prepared with K_2CO_3 activation. *SN Appl Sci* 2(4):702–709. <https://doi.org/10.1007/s42452-020-2465-1>
62. Chu B, Amano Y, Machida M (2020) Preparation of bean dreg derived N-doped activated carbon with high adsorption for Cr(VI). *Colloids Surf A Physicochem Eng Asp* 586:124262. <https://doi.org/10.1016/j.colsurfa.2019.124262>
63. Chu B, Terao K, Amano Y, Machida M (2020) Adsorption behavior of Cr(VI) by N-doped biochar derived from bamboo. *Water Pract Technol* 15(1):170–181. <https://doi.org/10.2166/wpt.2020.008>
64. Yoo P, Amano Y, Machida M (2020) Investigating the effective carbon material for thermal chemical vapor deposition using aniline to enhance as(V) adsorption capacity of activated carbon. *SN Appl Sci* 2:1179. <https://doi.org/10.1007/s42452-020-2974-y>
65. Yoo P, Amano Y, Machida M (2020) Effective preparation of nitrogen-doped activated carbon by aniline thermal chemical vapor deposition for arsenate adsorption. *Environ Eng Res* 25(5):707–713. <https://doi.org/10.4491/eer.2019.217>
66. Peng Z, Xiong C, Wang W, Tan F, Xu Y, Wang X, Qiao X (2017) Facile modification of nanoscale zero-valent iron with high stability for Cr (VI) remediation. *Sci Total Environ* 596:266–273. <https://doi.org/10.1016/j.scitotenv.2017.04.121>